Error Propagation and Uncertainty Analysis in a Virtual Patient Model for Lung Mechanics

Qianhui Sun[*], J. Geoffrey Chase[**], Cong Zhou[**], Thomas Desaive[*]

[*] *GIGA-In Silico Medicine, University of Liège, Liège, Belgium (e-mail: qianhui.sun@uliege.be; tdesaive@uliege.be)*

[**] *Department of Mechanical Engineering; Dept of Mechanical Eng, Centre for Bio-Engineering, University of Canterbury, Christchurch, New Zealand (e-mail: geoff.chase@canterbury.ac.nz; cong.zhou@canterbury.ac.nz)*

Abstract:

Background: Predictive models can offer significant aid in optimizing patient care. However, physiological models are imperfect due to errors or biases in modeling, identification, and/or the data used to personalize them. Data collection, model identification, and model prediction can all include inevitable errors and uncertainties which propagate and impact model prediction. Error propagation and uncertainty analysis are helpful for understanding model development, and yield insights into model design and potential improvement.

Methods: A well-validated predictive lung mechanics model is analyzed step-by-step through model identification and prediction to analyze four different types of uncertainties from input data, parameter estimation, model structure, and prediction. Propagated errors are analyzed as well. Data from 18 volume-controlled ventilation patients undergoing a staircase recruitment maneuver is used to assess overall prediction error for peak-inspiratory pressure (PIP) at different levels of positive end expiratory pressure (PEEP).

Results: Uncertainties for three segments of a pressure-volume (P-V) loop during inspiration and associated PIP prediction errors indicate error cancellation occurs as overall error is lower than the sum of each specific error. It arises partially from differently signed errors cancelling during propagation and partially due to model structure. Model structure plays an important role in overall model performance robustness and cannot be isolated and analyzed alone.

Conclusion: To develop an effective physiological model, moderate simplification while retaining physiologically relevant features is necessary to ensure model identifiability and robustness. Errors and uncertainties arise from the combination of model structure and error propagation in identified model predictions. In the nonlinear mechanics model analyzed, these errors tend to be cancelled leading to lower overall prediction errors. Overall, physiological models used to guide care are increasing and should examine specific sources of error propagation and their impact on overall outcome prediction error to better understand the causes. The approach presented provides a generalizable overall template for such analyses.

Keywords: Error propagation, Uncertainty analysis, Predictive model, Lung mechanics, Mechanical Ventilation, Virtual patient.

1 Introduction

Predictive models have been studied in mechanical ventilation (MV) and other medical areas for over 20 years, aiming to provide better, safer, and personalized care for patients and lower the burden on clinicians and hospital costs [1–3]. For MV, accurate predictions can be used to test new ventilator settings and reduce unintended harm to alveoli by testing and avoiding unnecessary and/or inappropriate settings [4,5]. An effective predictive model should be identifiable, capture physiologically-relevant patient-specific metrics, and provide accurate predictions of patient-specific response to treatment changes.

Some lung mechanics models successfully capture lung mechanics and dynamics at varying levels of complexity [6–17], as summarized in [18,19]. Models with higher complexity, such as multi-scale and finite element models, can simulate biomechanical behavior at the alveolar level with precise boundary conditions or medical images [20,21]. Simpler models requiring less computer power are more appropriate and thus more practically identifiable and thus efficient to estimate and identify lung function parameters with limited and rapidly changing data [1,18,20,22–24]. However, accurate predictions are more difficult and relatively far fewer studies accurately predict patient-specific pressure and volume responses to changes in MV care [25–29].

To develop an effective lung mechanics model to guide MV, the first issue is to determine the input data available, and, given these inputs, the features are able to be identified relative to clinical goals [19,22]. To personalize models, patient-specific features and model parameters are identified from data, and thus identification uncertainty occurs mainly due to the natural variability of patients, as well as the combination of model structure, identification method, and error in measured data [30,31]. Identified patient-specific model parameters can be used to generate model output predictions for any given change in care, where structural errors arise yielding inaccurate predictions due to model assumptions and complexity [30,32,33]. Overall, in this process, errors and uncertainties are integrated and propagated, and eventually, in combination, impact model prediction accuracy.

Uncertainties and errors exist everywhere in biomedical modelling [34–36] and similar biological and environmental modeling [33,37–39]. Given model complexity, errors and uncertainties are not simply added up or calculable in a simple way. Usually, the interactions of measurement, computational, and identification errors can be complex, even in a relatively simple model. Meanwhile, prediction accuracy and modelling errors may not act in proportional relationship and/or errors may cancel yielding a more accurate appearing total or overall prediction, despite larger, potentially unrealistic or non-physiological internal errors. Currently, uncertainty analysis and error propagation research in lung modelling field is commonly complicated and more interested in complex models, analyzing the robustness of the developed model and error source which thus can improve the model design and its application in practice [21,40–44]. For simpler models, less research is found due to only a few studies capable of delineating error sources in lung mechanics models [25–29].

The main goal of this study is to show the progress and contributions of error propagation for a well-validated predictive virtual-patient lung mechanics model [25,26,28], and to investigate the influence and significance of each of the modelled variables on model outcome prediction. In particular, the effects for each type of error and uncertainty are delineated to assess where errors may be large, small, or cancel, as well as thus delineating the sensitivity of identified variables on model predictions as a function of input data and model structure.

2 Methods

2.1 Uncertainty types

There are 4 types of uncertainty considered: Type 1: input data uncertainty in measuring physiological variables [45], and includes measurement error and data noise, which is from clinical data in this work; Type 2: parameter uncertainty, which is caused by estimation (identification) from natural variation in systems [30,45] and usually increases as the degree of model simplification increases, such as the error yielded in a curve-fitting procedure; Type 3: structural uncertainty, the errors yielded by chosen model structure, which interacts with other errors in yielding overall model prediction performance [33]; and finally Type 4: outcome prediction uncertainty or error, yielded by the prediction functions, such as basis functions [25,27,29], and/or model applied. This analysis is applied to a nonlinear model of lung mechanics used to predict outcome patient response to input changes in MV care [25,26,28].

2.2 Uncertainty analysis in hysteresis lung mechanics (HLM) model

2.2.1 HLM model and relevant uncertainties

The HLM lung mechanics model has demonstrated overall high accuracy levels in predicting clinically relevant peak pressures and volumes in MV including distension risk [25,26,28]. It is adapted to respiratory pressure-volume (PV) loop analysis [26,28,46,47]. This study uses the same prediction basis functions, model, and clinical trial data in [26].

Uncertainties in identified parameters and output predictions are influenced by model structure, defined [26,28]:

$$f_V(t) + PEEP = \ddot{V} + R\dot{V} + K_e V + K_{h1} V_{h1} + K_{h2} V_{h2} \quad (1)$$

where $f_V(t)$ is the steady-state input force, which is the driving pressure for applied breath, $P(t) - \text{PEEP}$. $P(t)$ is the airway pressure waveform. PEEP is the positive end-expiratory pressure. V is the volume of air delivered to the lungs, V_{h1} and V_{h2} are hysteretic volume response during inspiration and expiration, respectively. R is the

airway resistance. K_e represents the alveolar recruitment elastance, named $k2$ in this approach. K_{h1} and K_{h2}, are determined by two nonlinear hysteretic springs for alveolar hysteresis elastance during inspiration and expiration, respectively, which are calculated with identified elastances. The detailed formulations for calculating and identifying each parameter can be found in [28].

Measured model input data comprises airway pressure and flow, and can be defined:

$$Data_{input} = \{P(t, e_p), Q(t, e_q), PEEP\} \tag{2}$$

Where e_p and e_q , Type 1 errors, are the random deviation from measured trajectories of airway pressure and flow, *P(t)* and *Q(t)*. Volume, *V(t)*, is the single integral of flow, *Q(t)*, over time.

This measured nonlinear P-V loop is broken down and identified as linear segments (**Figure 1**), where this linear approximation is calculated with its own parameter/variable uncertainties:

$$Var = Var_{optimal} + e_{var} \tag{3}$$

Where Var represents all involved parameters and variables input into HLM. $Var_{optimal}$ are the optimal values, which only exist in ideal and theoretical situations. No model is perfect, especially in physiological modelling. Hence, Type 2 error, e_{var}, the deviation for parameters/variables by identification caused by natural variability and possible random deviation, i.e. Type 1 errors (e_p and e_q) from input data (Equation 2), exists.

Once all required data are put into the HLM to identify the model and then reconstruct the P-V loop, structural model uncertainty, Type 3 error, arises. Model output thus can be generated by combining Equations (1)-(3):

$$f_V(t)_{output} = f_V(Data_{input}, Var) + e_{se} \tag{4}$$

$$e_{output} = f_V(e_p, e_q, e_{var}) + e_{se} \tag{5}$$

Where e_{se} is the structural uncertainty, Type 3 error. $f_V(t)_{output}$ is the actual model output. e_{output} is the yielded error in model output.

Finally, model outputs can be predicted for any change of input parameters related to care, yielding an outcome prediction uncertainty, Type 4 error. In particular, the identified HLM model is used to generate and predict a P-V loop for a new set of MV settings or inputs. This prediction has errors related to all these uncertainties. **Table 1** summarizes all the parameters and variables involved.

Table 1: Involved variables/parameters in HLM. All the variables and parameters can be found in Figures 1-2. The prediction functions can all be found in the previous published work [26]. Subscription 'i' indicates the predicted values, and '1' indicates the identified value at baseline PEEP level.

Variables /Parameters	**Property**	**Prediction/Calculation equations**
P_{start}	Estimated	$= P_{start-1} + \Delta PEEP$
k1	Keep constant	Identified at baseline PEEP level, and no predictions
V_{LIP}	Predicted, V_{LIP-i}	$= V_{LIP-1} * \left(\min\left(\frac{P_r}{PEEP_{max}}, \frac{PEEP_{max}}{P_r}\right) - \left(\frac{\Delta PEEP}{PEEP_{max}}\right)^2 \right)$ Where $P_r = \max(P(t)) - \min(P(t))$ at baseline $PEEP_1$, and $PEEP_{max}$ = 24 cmH_2O
P_{LIP}	Yielded by P_{start}, *k1*, V_{LIP}	$= k1 * V_{LIP-i} + P_{start}$
k2	Predicted, $k2_i$	$= \left(\frac{PEEP_i}{k1} + \frac{k2_1}{k1} * e^{b * \frac{PEEP_i}{k1}}\right) * k1$ Where $b = \frac{k1}{PEEP_1} * \log\frac{k2_1 - PEEP_1}{k2_1}$
V_{UIP}	Keep constant	Identified at baseline PEEP level, and no predictions
P_{UIP}	Yielded by LIP position, V_{UIP}, predicted *k2*	$= k2_i * (V_{UIP} - V_{LIP}) + P_{LIP}$
k2end	Predicted, $k2end_i$	$= \left(\frac{PEEP_i}{k2_i} + \frac{k2end_1}{k2_1} * (\theta 1 + (\Delta PEEP * \theta 2)^2)\right) * k2_i$ Where $\theta 1 = \frac{k2end_1 - PEEP_1}{k2end_1}$, $\theta 2 = \frac{EELV_1}{PIV_1 - EELV_1}$
V_{PIP}	Keep constant	Identified at baseline PEEP level, and no predictions
P_{PIP}	Yielded by UIP position, V_{PIP}, predicted *k2end*	$= k2end_i * (V_{PIP} - V_{UIP}) + P_{UIP}$

The significance of the influence and interaction complexity among all involved parameters/variables may differ from model to model. To give a clear idea on how HLM works, and the relative parameters/variables involved in each step, a real example of the entire identification and estimation procedure is presented step by step in **Figure 1**. The identified patient-specific model prediction process is shown in **Figure 2**.

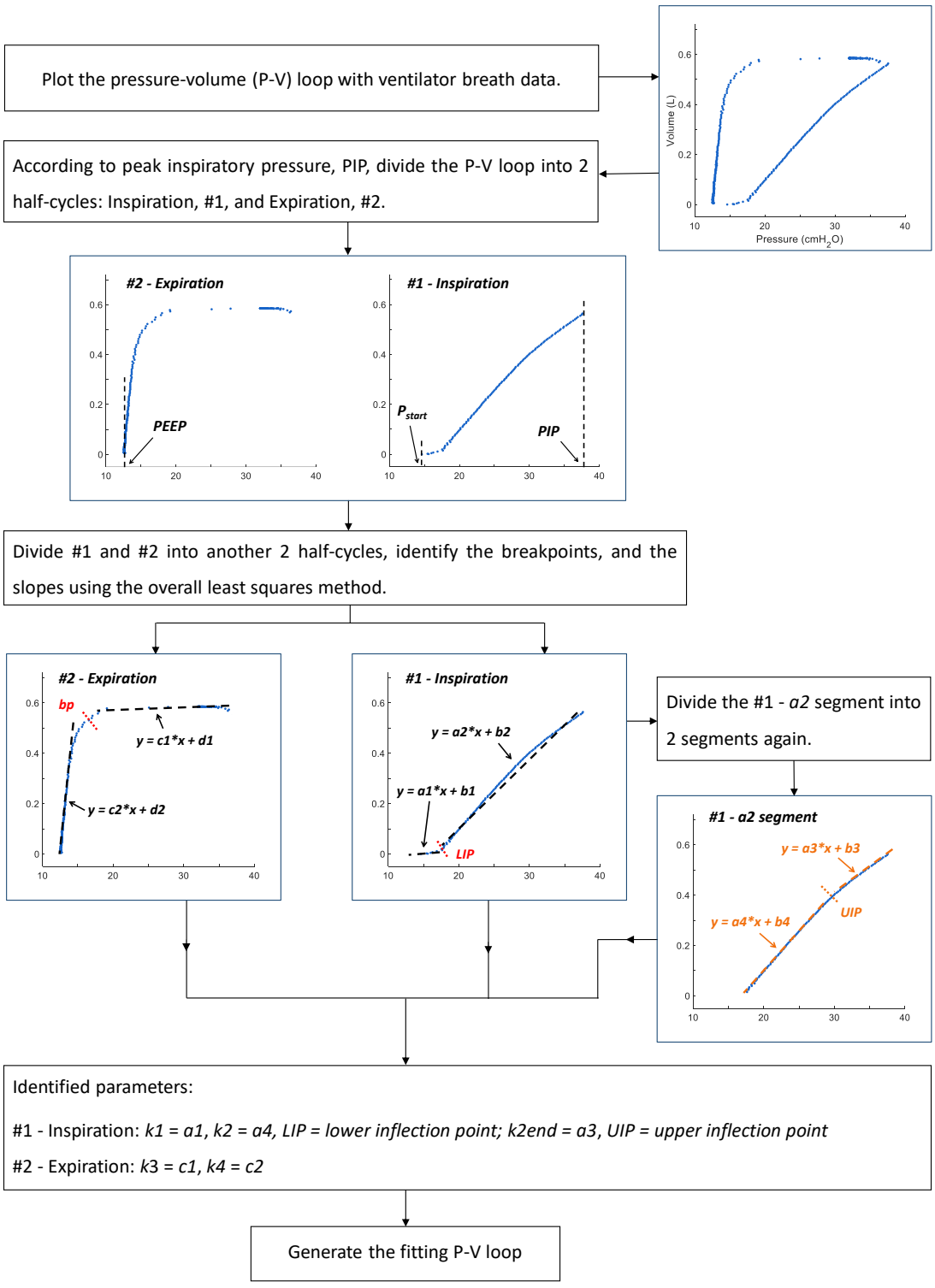

Figure 1: Identification flowchart step by step. Blue dots are the clinical P-V loop, while other straight dashed lines are identified elastances. PIP = peak inspiratory pressure. PEEP = positive-end-expiratory-pressure.

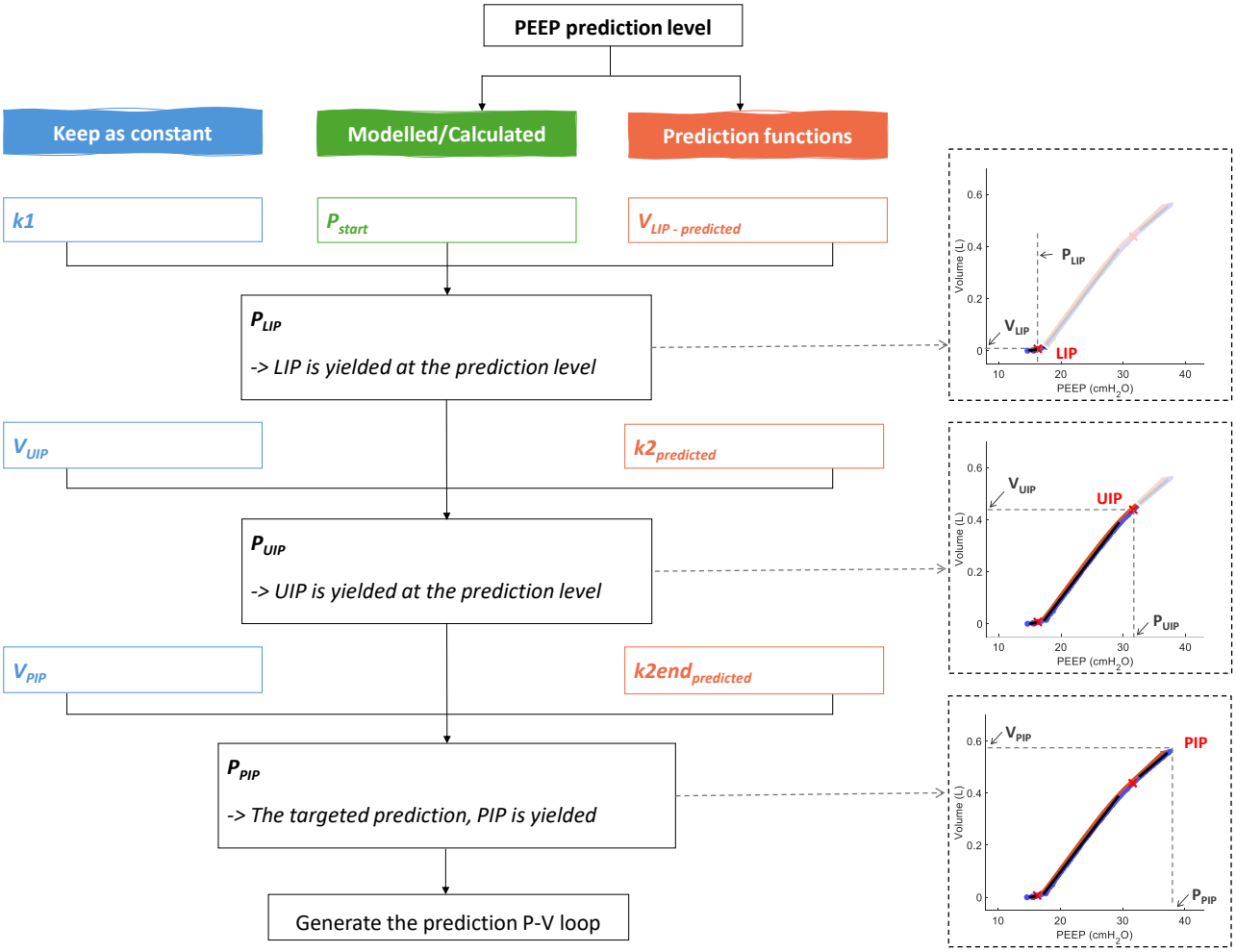

Figure 2:Prediction flowchart step by step. Blue dots and black straight lines are clinical data and identified elastances. Orange lines are the generated prediction P-V loop.

2.2.2 Uncertainty analysis

Uncertainties exist in every step of identification and prediction presented in **Figures 1-2**. The data adopted in this study is from volume-controlled ventilation (VCV), where the delivered volume (flow) is under control and the resulting pressure arising from this input is unknown. Hence, the pressure differences in PIP, or ΔPIP, are the final prediction errors.

To analyze the errors propagation and the error contribution for final model output in the prediction procedure, the inspiration phase can be simplified with global coordinates and defines the P-V loop starting point, (P_{start}, V_{start}), to be the origin, (*0, 0*), as shown in **Figure 3**. This figure shows the separate segments and sets relative coordinates for use in later analysis. The three segments noted and their resulting points all may have overall errors from the interaction of all four error types, which are not separable.

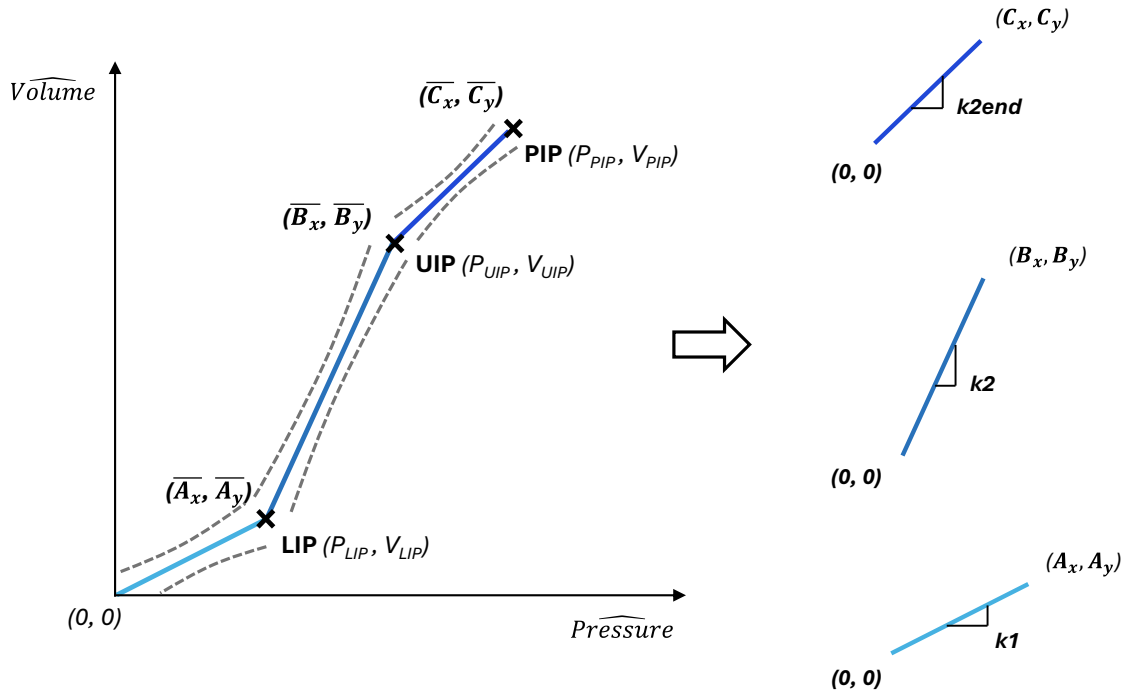

Figure 3: Inspiration phase simplification with global coordinates and the 3 separate segments with relative coordinates. Dashed lines are the schematic illustrations of the confidence ranges due to all forms of error, which sum to resulting errors in lower and upper inflection points (LIP and UIP) and along the segments. The error of each segment can be addressed individually and then propagated to a sum.

Using **Figure 3**, for each segment, the uncertainty in any prediction (**Table 1**) of the main coordinates can be calculated:

$$\Delta A_x = \pm(P_{LIP-clinical} - P_{start})\sqrt{\left(\frac{V_{LIP-predicted} - V_{LIP-clinical}}{V_{LIP-clinical} - V_{start}}\right)^2 + \left(\frac{k1_{fixed} - k1_{clinical}}{k1_{clinical}}\right)^2} \quad (6)$$

$$\Delta B_x = \pm(P_{UIP-clinical} - P_{LIP-clinical})\sqrt{\left(\frac{V_{UIP-fixed} - V_{UIP-clinical}}{V_{UIP-clinical} - V_{LIP-clinical}}\right)^2 + \left(\frac{k2_{predicted} - k2_{clinical}}{k2_{clinical}}\right)^2} \quad (7)$$

$$\Delta C_x = \pm(P_{PIP-clinical} - P_{UIP-clinical})\sqrt{\left(\frac{V_{PIP-fixed} - V_{PIP-clinical}}{V_{PIP-clinical} - V_{UIP-clinical}}\right)^2 + \left(\frac{k2end_{predicted} - k2end_{clinical}}{k2end_{clinical}}\right)^2} \quad (8)$$

Where V_{start} = 0 L. ΔA_x, ΔB_x, and ΔC_x represent the segment uncertainties for segments *k1*, *k2*, and *k2end*, respectively. $\overline{A_x}$ and $\overline{A_y}$ are the coordinates for $LIP_{clinical}$; $\overline{B_x}$ and $\overline{B_y}$ are $UIP_{clinical}$; $\overline{C_x}$ and $\overline{C_y}$ are $PIP_{clinical}$ in a real P-V loop.

Combining Equations (6)-(8) yields:

$$\Delta PIP_x \approx \pm\sqrt{\Delta A_x^2 + \Delta B_x^2 + \Delta C_x^2} \quad (9)$$

Where ΔPIP_x represents the propagated PIP error calculated by Equations (6)-(8). Note, ΔPIP_x error only considered error propagation effect, while ignoring the error cancellation by signs of ΔA_x, ΔB_x, and ΔC_x. However, as stated in Equations (6)-(8), they all are ± values.

Elastance identification quality and prediction errors are analyzed in relation to segment uncertainty from Equations (6)-(9) and model output (ΔPIP). A brief comparison and discussion about modelled parameters/variables versus the real ones for model performance is also provided. The examined baseline PEEP levels are set to be 10 cmH_2O for all patients, while prediction levels are at 8 cmH_2O (backwards prediction), and 12 cmH_2O (forward prediction). The prediction functions from **Table 1** are applied for both backwards and forwards predictions, where the backwards predictions are first introduced and are different from previous work, which considered only forward predictions to higher PEEP. However, in both directions, the prediction method remains the same.

2.2.3 Study Design and Workflow

First, the error introduced from each segment (*k1*, *k2*, and *k2end* segments) during prediction for model output is analyzed and compared to study the error cancelation and give a general look for error propagation with Equations (6)-(9) in Section 3.1. Then, as shown in **Figure 3**, the three segments contain three elastances (*k1*, *k2*, and *k2end*) separated by two turning points (LIP and UIP). The elastance prediction errors are thus analyzed to study the contribution to the segment errors in Section 3.2.

Then variables are grouped into 3 types during prediction (as stated in **Figure 2**): keeping as constant, modelled/calculated, and predicted with functions. The comparison of model output, PIP errors, is analyzed as

the standard to evaluate whether real clinical variables or model-defined/predicted variables are more appropriate in Section 3.3. Finally, all results will be discussed from the perspective of model design and performance optimization.

2.3 Patient data

The McREM trial was conducted across eight German university ICUs from September 2000 to February 2002 [48]. Airway pressure and flow data are collected via Evita4Lab systems (Draeger Medical, Lübeck, Germany) and sampled at 125 Hz. Patients were ventilated under VCV with square shape flow waveform while tidal volume was targeted at 8±2 mL/kg body weight. All patients were ventilated in the supine position while sedated to achieve a Ramsay sedation score of 4–5 [48].

Each patient in McREM underwent one incremental staircase recruitment maneuver (RM) via 2cmH_2O steps starting from PEEP = 0 cmH_2O (ZEEP). Patient demographics are provided in the online Appendix, while all patients have some level of ARDS, as defined by PaO_2/FiO_2 (P/F) ratio, P/F < 300 mmHg [49]. During ventilation, an end-inspiratory hold ≥ 0.2 s is applied for each breath. The number of PEEP levels applied for each patient varies from 6 to 14 steps, yielding a total of 196 cases (PEEP steps) with maximum PEEP ranging over 10-26 cmH_2O [48]. With PEEP settings explained in Section 2.2, the examined PEEP levels yield a total number of 36 cases in prediction and 18 cases in identification. Patient 19 is excluded for the insufficient PEEP levels to keep consistent with others (highest PEEP = 10 cmH_2O).

The patients in this study all have relatively low P/F ratios due to ARDS or severe ARDS. Thus, the P-V loops are representative of this cohort and may vary in patients with less severe ARDS who are nonetheless under invasive MV for other reasons. If these other patients have distorted P-V loops due to this difference in condition, then the methods may not be as applicable. However, prior work [25,26,28] shows the ability to capture a wide range of P-V loops, including asynchrony [47]. Thus, we are confident we can capture the full range of patient behaviors, but would require a more comprehensive study to confirm this outcome.

3 Results

3.1 Uncertainty in three segments, *k1*, *k2*, *k2end*

Figure 4 presents the uncertainties for 3 segments calculated with Equations (6)-(8) and the comparison to ΔPIP_x errors from Equation (9) when predicting PIP at a PEEP of 12 cmH_2O from a model identified at PEEP of 10 cmH_2O. The comparison with model-yielded PIP errors shows the error propagation and cancellation due to sign of the errors and the influence of model structure for most of the patients. The larger the difference between ΔPIP_x and model-yielded PIP prediction error, the larger the error cancelation exists. Note, all errors are presented in absolute values (positive) for clearer visualization but are all signed errors per Equations (6)-(9), as well as for the actual model-yielded PIP errors. **Figure 5** presents the same data at the "backward" prediction to a PEEP = 8 cmH_2O from the same identified model at PEEP = 10 cmH_2O.

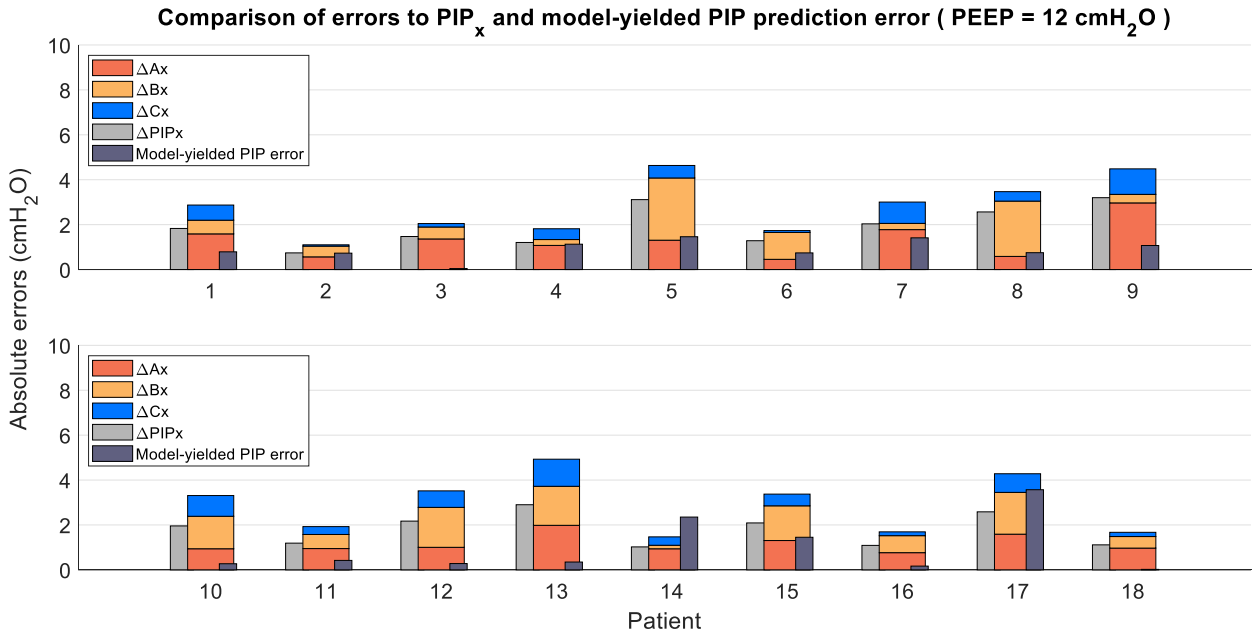

Figure 4: Error propagation and the comparison of ΔA_x, ΔB_x, and ΔC_x to PIP_x errors, while real PIP model-yielded error shows the error cancellation from the signed prediction errors and model structure. All presented errors are absolute. PEEP is at a forward prediction level of 12 cmH_2O.

Figure 6 shows the predicted P-V loops at 12 cmH_2O for Patients 13 and 17 with similar ΔA_x, ΔB_x, and ΔC_x comparison and PIP_x. However, Patient 17 yields a much larger PIP error than Patient 13, -3.57 cmH_2O compared to 0.35 cmH_2O. The PIP error for Patient 17 mainly results from inaccurate LIP position and *k2end*

elastance prediction undershoot as shown. Patient 17 also had the lowest P/F ratio = 75 mmHg < 100 mmHg (considered as severe acute respiratory distress syndrome, ARDS [49]) versus P/F ratio = 143-298 mmHg (mild to moderate ARDS [49]) for the others, which may be more indicative of the patient condition than of the model structure. Detailed patient demographic and diagnostic information is available in the supplemental Appendix.

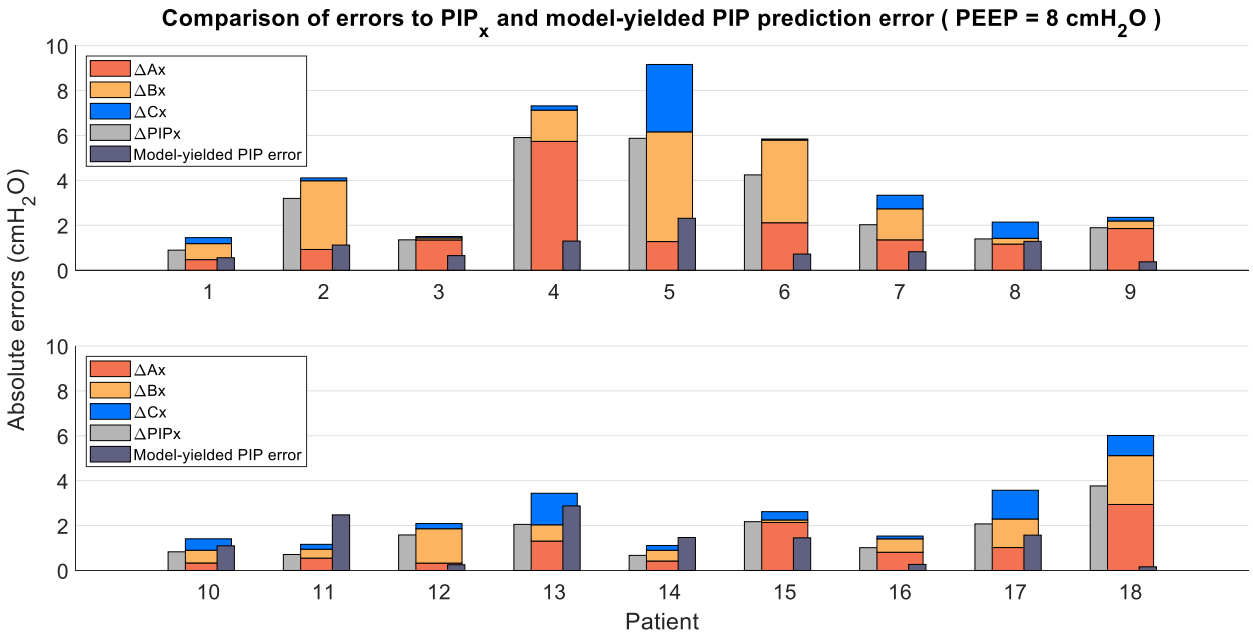

Figure 5: Error propagation and the comparison of ΔA_x, ΔB_x, and ΔC_x to PIP_x errors, while real PIP model-yielded error shows the error cancellation from the signed prediction errors and model structure. All presented errors are absolute. PEEP is at a backward prediction level of 8 cmH_2O.

Patient 9 and Patient 8 are the other comparison in **Figure 6** with similar PIP error while ΔA_x and ΔB_x are the main contribution to PIP_x for each, 66% and 71%, respectively. For Patient 9, the larger ΔA_x originates from the relatively larger V_{LIP} prediction error and *k1* elastance value used. Meanwhile, the *k2end* prediction is suboptimal as well and thus enlarges the PIP error. In contrast, the V_{LIP} and *k1* predictions are better in Patient 8, and the *k2* predictions are similar.

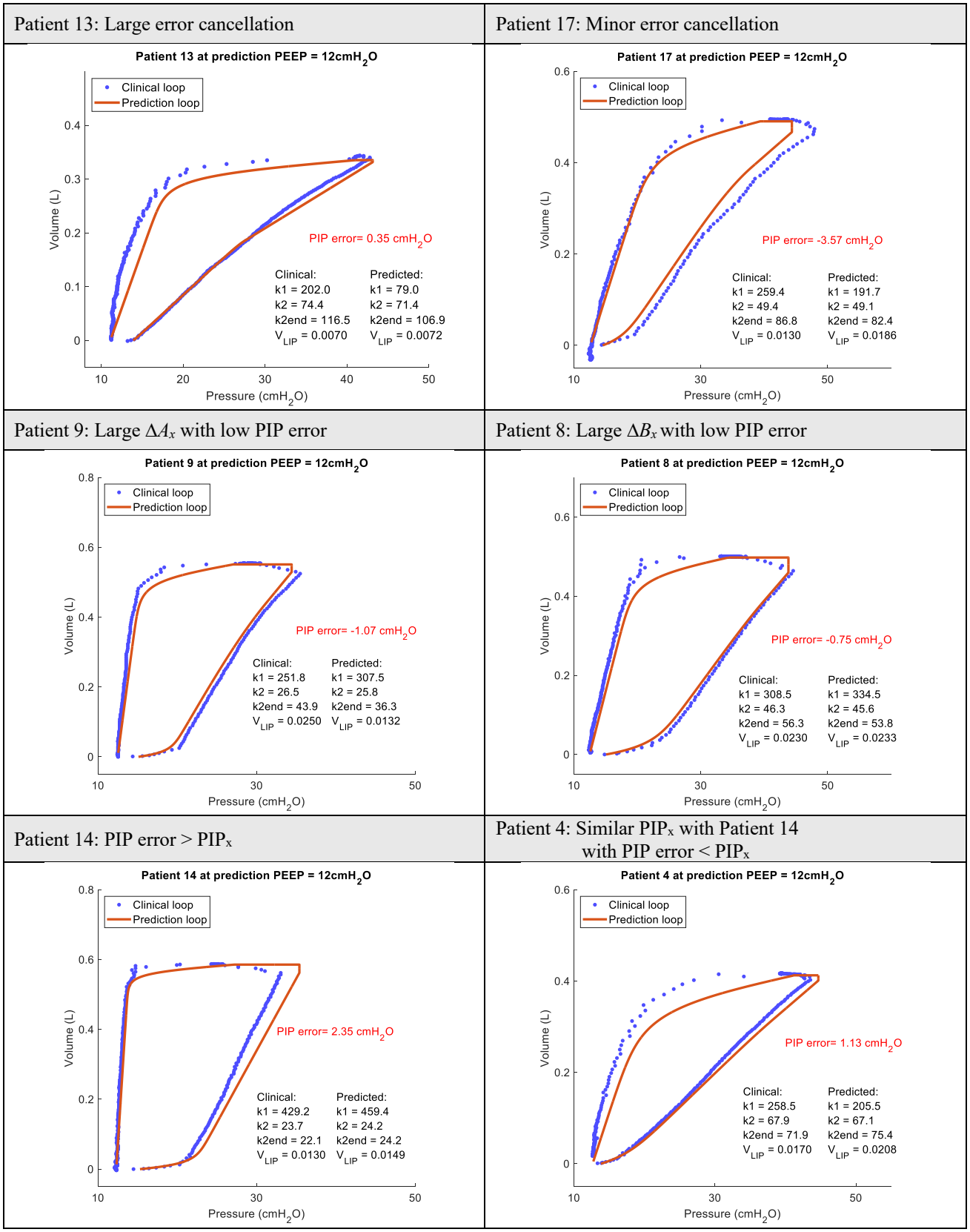

Figure 6: Predicted P-V loops for (upper panel) Patients 13 and 17 for large and minor error cancellation comparison; (middle panel) Patients 8 and 9 for similar PIP errors where the PIP_x is mainly contributed by ΔB_x and ΔA_x, respectively; (lower panel) Patients 4 and 14 are with similar ΔA_x, ΔB_x, and ΔC_x, while Patient 4 is observed with error cancellation benefits and Patient 14 is with no error cancellation. The related key variables (clinical/identification and prediction values) are provided, while units are omitted.

Patient 14 is observed with real PIP error greater than PIP_x for forwards prediction at PEEP = 12 cmH_2O, where all four key predictions are overestimated. To compare, the similar proportion of ΔA_x, ΔB_x, and ΔC_x (so is ΔPIP_x) are yielded in Patient 4. However, the underestimated *k1* elastance largely compensates the overshoot of V_{LIP} and *k2end* elastance and thus result in a lower PIP error, 1.13 cmH_2O compared to 2.35 cmH_2O in Patient 14. At prediction level PEEP = 8 cmH_2O, backwards prediction in **Figure 5**, Patients 11 has a noticeable PIP_x > PIP prediction error, which resulted by overestimated *k2* value. The prediction P-V loops for all 18 patients at both PEEP levels are attached to the supplemental Appendix.

3.2 Variable uncertainties

Figures 7-8 compare signed elastance prediction errors (%) for each limb of the inspiratory P-V loop in **Figure 3** with the margin of error (±Δ, in percentage) and the model-yielded PIP prediction error (%) for the forward prediction to PEEP = 12 cmH_2O and backward prediction to PEEP = 8 cmH_2O from PEEP = 10 cmH_2O, respectively. **Table 2** provides the three elastance, *k1*, *k2*, and *k2end*, identification outcome at PEEP = 10 cmH_2O. The margins of error are all calculated as the 95% confidence interval. Matched with **Figures 4-5**, *k1* segment yields the largest uncertainty and low precision for *k1* elastance identification. In contrast, the elastance identification average errors are ±1.5% for *k2* (excluding Patient 7) and 3.4% for *k2end*, as shown in Table 2.

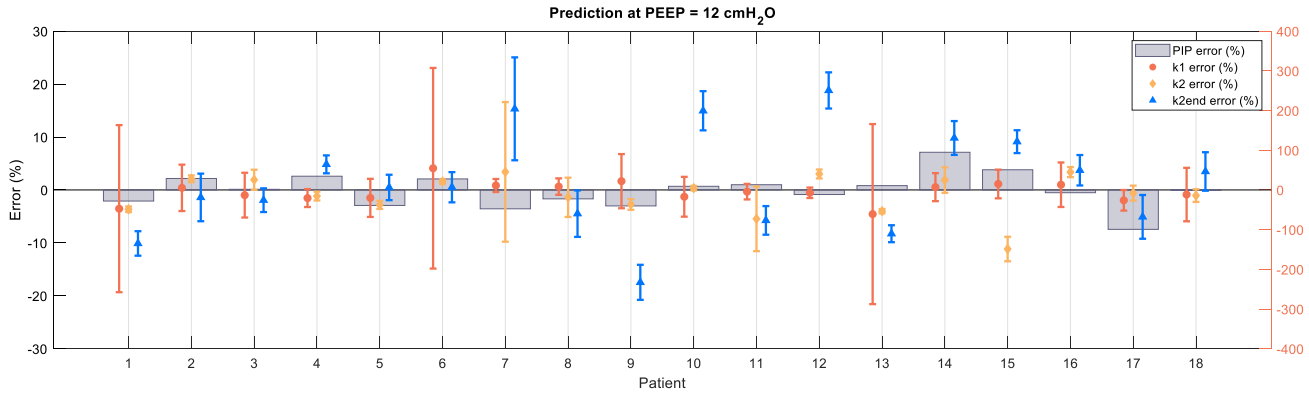

Figure 7: Elastance prediction errors (%) with margin of error are compared with PIP prediction error (%) yielded by model. Note the y-axis of *k1* errors is on the right. Prediction level at PEEP = 8 cmH_2O (backwards).

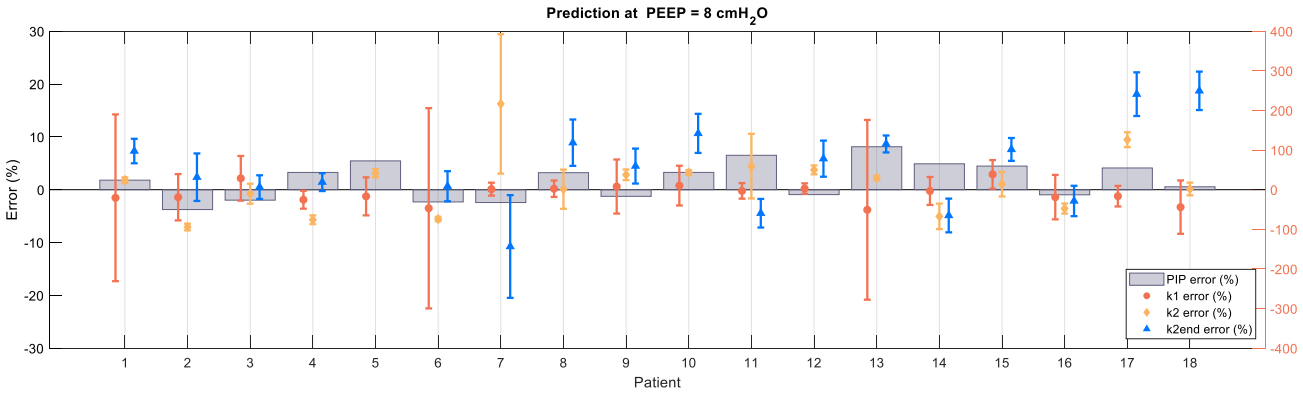

Figure 8: Elastance prediction errors (%) with margin of error are compared with PIP prediction error (%) yielded by model. Note the y-axis of *k1* errors is on the right. Prediction level at PEEP = 12 cmH_2O (forwards).

Table 2: The elastances *k1*, *k2*, and *k2end* (cmH_2O/L) identified at PEEP = 10 cmH_2O and the margin of error (±Δ, in value and percentage) of confidence interval = 95%.

	k1			*k2*			*k2end*		
	value	±Δ	±Δ (%)	value	±Δ	±Δ (%)	value	±Δ	±Δ (%)
Patient 1	135.3	284.8	210.5%	30.3	0.16	0.5%	42.1	0.97	2.3%
Patient 2	288.7	168.7	58.4%	17.5	0.11	0.6%	22.2	1.00	4.5%
Patient 3	327.5	184.6	56.4%	37.0	0.70	1.9%	39.3	0.88	2.2%
Patient 4	205.5	46.4	22.6%	66.9	0.56	0.8%	72.8	1.23	1.7%
Patient 5	379.2	182.0	48.0%	40.9	0.31	0.8%	65.1	1.56	2.4%
Patient 6	272.6	688.9	252.7%	25.2	0.10	0.4%	29.6	0.84	2.9%
Patient 7	407.2	66.7	16.4%	12.9	1.70	13.2%	26.2	2.55	9.7%
Patient 8	334.5	69.3	20.7%	45.3	1.68	3.7%	51.4	2.26	4.4%
Patient 9	307.5	209.8	68.2%	25.2	0.25	1.0%	33.8	1.12	3.3%
Patient 10	646.3	324.2	50.2%	24.2	0.10	0.4%	38.9	1.44	3.7%
Patient 11	421.8	82.6	19.6%	19.1	1.16	6.1%	18.8	0.51	2.7%
Patient 12	301.9	39.8	13.2%	15.1	0.13	0.8%	19.4	0.66	3.4%
Patient 13	79.0	179.2	226.8%	71.2	0.29	0.4%	104.2	1.67	1.6%
Patient 14	459.4	162.1	35.3%	23.5	0.57	2.4%	21.7	0.69	3.2%
Patient 15	416.1	150.4	36.1%	21.9	0.51	2.3%	24.9	0.54	2.2%
Patient 16	231.9	130.0	56.1%	33.7	0.32	1.0%	37.9	1.09	2.9%
Patient 17	191.7	49.7	26.0%	48.8	0.69	1.4%	78.2	3.23	4.1%
Patient 18	211.6	142.5	67.4%	34.1	0.41	1.2%	46.4	1.69	3.6%

3.3 Modelled variables vs clinical variables

Figure 9 shows an example of the influence of V_{LIP} values in **Figure 3** on final PIP predictions with predicted and clinical values. First, the error differences are minor as expected given on the small values of V_{LIP}, showing the robustness of HLM model at the meantime. Second, V_{LIP} predictions are good in this patient for backward

prediction to PEEP = 8 cmH_2O, with an error within 2%. However, for forward prediction to PEEP = 12 cmH_2O, the PIP error is unexpectedly smaller with predicted V_{LIP} instead of the real, clinical value (0.003 L in prediction difference, 38.5% in percentage error), which appears large due to the very small value of volume.

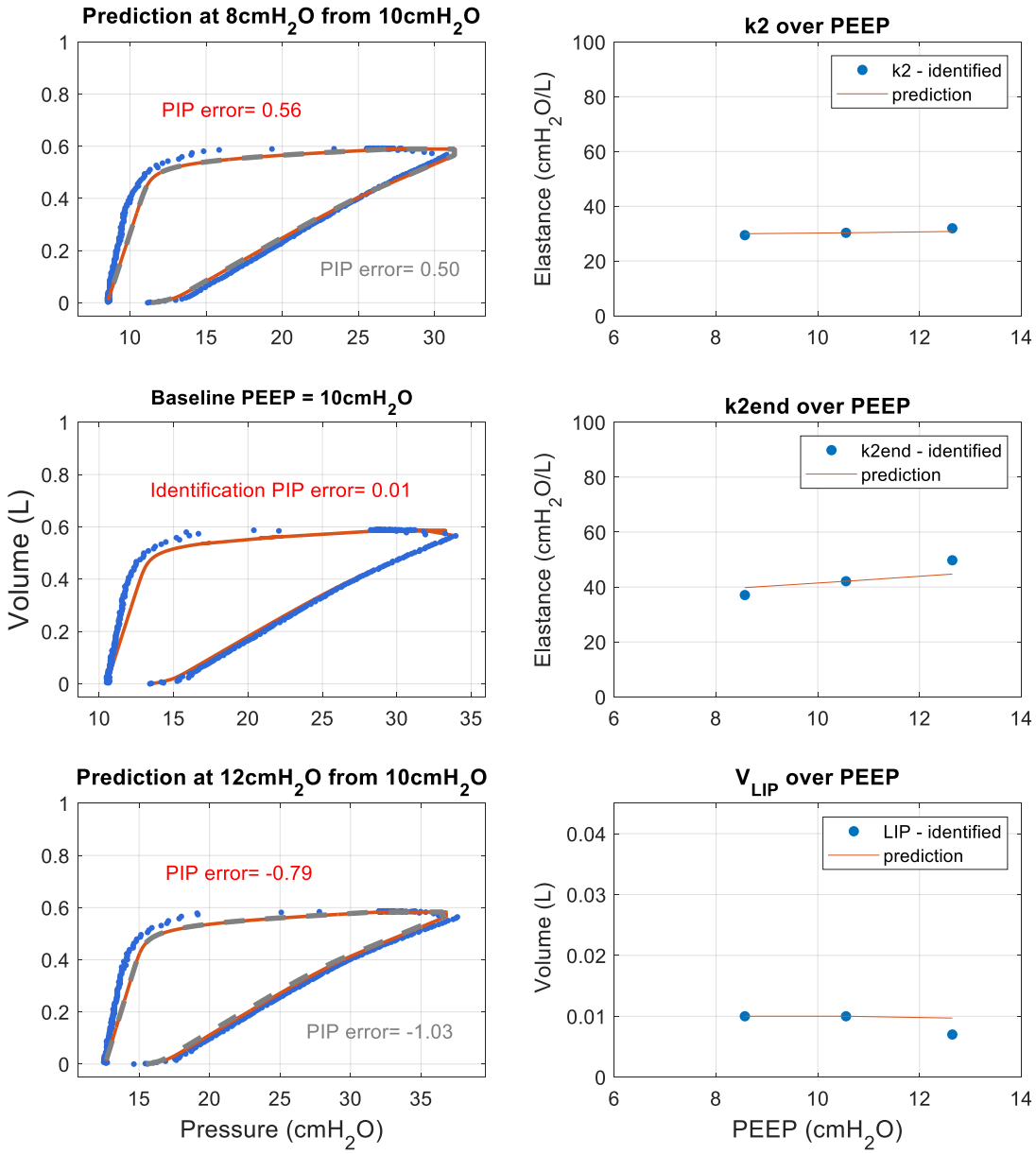

Figure 9: Examples for PIP prediction error (cmH_2O) comparison using clinical and predicted V_{LIP} over PEEP. The contrast for identified and predicted variables of *k2*, *k2end*, and V_{LIP} are also provided. Blue circles are the clinical P-V loop; orange cycles are predictions with predicted V_{LIP}; dashed grey cycles are predictions with clinical/identified V_{LIP} at the prediction level, while corresponding yielded PIP errors are noted in the same color. The second P-V loop on the left column is the identification case.

Figure 10 provides paired PIP prediction errors comparison for all 18 patients at the 2 prediction levels. It can be generally seen the prediction performance is more stable and better with predicted/modelled V_{LIP} other than

using the real, clinical values. It is necessary to note the LIP is affected by V_{LIP}, elastance *k1*, and P_{start} jointly, while only V_{LIP} is predicted (**Table 1**).

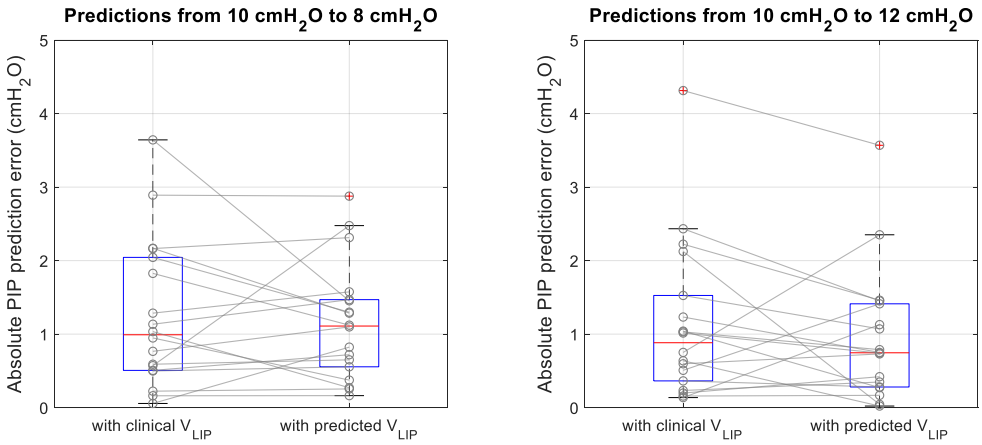

Figure 10: Boxplot for paired PIP prediction errors comparison between clinical (left boxes) and predicted (right boxes) V_{LIP} from a PEEP of 10 cmH_2O to (left panel) 8 cmH_2O and (right panel) 12 cmH_2O.

4 Discussion

In Section 3.1, the error propagation and the final yielded prediction outcome are presented and compared. Error cancellation and model structure play an important role for model output accuracy. In Sections 3.2, it shows this model structure also provides great robustness for the model output. PIP errors are small overall even with relatively large elastance prediction error. In Section 3.3, the modelled variables with error could be more beneficial for the model compared to real variables, especially if the real variable is from variable and unpredictable dynamics (**Figure 9**, V_{LIP} values over PEEP) in patient data.

4.1 HLM model design

The predicted P-V loop has smooth curvature at LIP and UIP in **Figure 6** because the HLM model and identification procedure assures the curvature at each turning point evolves to suit the input patient data at the baseline PEEP level (model training). The function is fulfilled by the novelty, intrinsic feature of the HLM model to which previously widely used in civil engineering to estimate the hysteresis response of structural system in earthquakes [50]. Then, the modelled curvature can compensate for the possible unideal identification due to any type of error, as in Equations (2)-(3). Furthermore, the curvature features can have more advantages in patients in other MV modes, such as pressure-controlled ventilation [25], enhancing the generality application of HLM in ventilation care.

In HLM, the nonlinear P-V loop is identified as multiple segments by design. Some research tried to do nonlinear identification/fitting for the P-V loop [51], or pressure or volume over time trajectories [52–54]. Similar efforts with similar loops in civil engineering have yielded poor results, as well [55]. Overall, the physiological phenomenon is not simple, and increased complexity in the model or its identification does not necessarily offer great improvement and comes at the risk of over-fitting.

The physiological curvature at each turning point influences spatial position of each segment in the identified model. In **Figure 6**, the much larger ΔB_x in Patient 8 could be generated from greater curvature at LIP during calculation, compared to the sharper turning curvature in Patient 9 with similar *k2* prediction accuracy. This

comparison shows how model structure in the form of the modelled P-V loop curvature stabilizes the model performance and thus the resulting PIP prediction. This influence can also be partly seen in the large uncertainty in *k2* segment (**Figure 4**), but smaller errors in its elastance predictions (**Figures 7-8** and **Table 2**), which are influenced by both LIP and UIP positions (Equation (7)).

Meanwhile, with increasing number of variables and parameters in the model, increased model complexity, lower tolerance of random errors, and physiological information losses are the more severe issues to solve [45]. Currently, a few nonlinear approaches can successfully capture patient-specific, physiologically relevant features [52], but have limitations for automatic application [46]. Currently, none of them offers prediction quality similar to the model used here.

4.2 Uncertainties

In this study, data uncertainties can be seen in **Figure 6**. A more variable inspiration phase can be observed in Patients 13 and 17 (Patients 2, 5, 7, 12, and 15 in the supplemental Appendix). Identification quality (parameter uncertainties) is thus affected, as shown in Table 2. *k1* elastance values are dramatically variable varying from 79.0 to 646.3 cmH_2O/L across patients with margin of error = 13.2% – 252.7%, within confidence interval = 95%. It is affected by data uncertainties and inherent characteristics in breath data jointly, where the latter is the main contribution. The segment of *k1* is the beginning of inspiration (breath) and thus can be the most unstable (and less linear) segment in a P-V loop. Meanwhile, it is a short segment which usually contains less than 10 data points ($\leq$0.08 seconds, sampling rate 125 Hz for the clinical trial studied) as airways fill rapidly with rapid pressure rise before recruiting significant lung volume. This short segment can also depend on specific ventilator pump dynamics. Therefore, the large uncertainties in this segment are reasonable as the identification is based on limited and sometimes noisy data.

Segment *k1* is much more variable compared to *k2* and *k2end* which naturally comes with large uncertainties due to breath dynamics characteristics. **Figure 10**, which shows the current applied prediction function for segment *k1* yields a robust performance in final PIP predictions, indicates for a simulation and prediction model

it may not be necessary to have extreme high accuracy for all model input variables, which in this case is an indication of this model's robustness. A similar situation arises with *k1* elastance, which currently keeps constant since identification (no prediction function). To conclude, the current prediction functions combined for *k1* and V_{LIP} (Table 1) with HLM model (curvature features) is validated to be effective and robust in prior works [26,56]. Hence, moderate simplification for required variables can enhance model robustness and performance.

In **Figure 4**, for 16 out of 18 patients at prediction level PEEP = 12 cmH_2O, the actual model prediction errors are noticeably lower than ΔPIP_x errors calculated by ΔA_x, ΔB_x, and ΔC_x in Equations (6)-(9). Meanwhile ΔA_x usually yields the largest and most variable uncertainty/error, with an average value of 1.23 cmH_2O (1.08 cmH_2O for ΔB_x and 0.55 cmH_2O for ΔC_x). ΔB_x is as variable as ΔA_x, while ΔC_x is relatively the most stable with the smallest errors. The possible reason for this performance could be the difficulty identifying and predicting the *k1* segment, as discussed previously, yielding large variations in the identified *k1* elastance and associated LIP position. Similar performance is observed in **Figure 5** for backward prediction at PEEP = 8 cmH_2O.

The spatial position of *k2* segment in the next step in prediction is subsequently influenced by this LIP position, *k2* elastance prediction, and thus UIP positions (**Table 1** and Equation (7)) which may see this error propagation as seen in ΔB_x. Further, the *k2end* segment at the end of the inspiratory limb of the P-V loop with lowest ΔC_x variation is impacted by the resulting UIP point as well. The end PIP error should not theoretically be larger than the sum in Equation (9), PIP_x, which holds for all but Patients 14 and 17. For Patient 14 shows minimal error cancelation while Patient 17 is more resulted by its severe condition (lowest P/F ratio) than other patients leading to less ideal prediction performance. The much lower errors for many patients indicate higher levels of error cancellation across these three errors and any added impact of model structure, which likely indicates an overall robustness in the model structure and identification / prediction methods.

Elastances *k2* and *k2end* have overall accurate predictions and a moderate confidence range, while the *k1* segment shows more uncertainty mostly due to limited segment samples which resulted by breath characteristics, as shown in **Figures 7-8** and **Table 2**. Given the model structure and prediction procedure (**Figures 1-2**) design,

the three segments and their prediction accuracy are jointly working on the model output, PIP predictions. Furthermore, error cancellation can be considered as a feature from model structure since it is not only generated by error signs but also spatial positions which could be influenced by HLM model. Hence, as shown in **Figures 4-5**, although structure uncertainty is not able to be isolated for analysis, the robustness of prediction and error cancellation are the indicators for low model structure uncertainty and strong model robustness and stability.

The whole procedure of identification and prediction and breaking nonlinear P-V loops into linear segments are the model simplification by choice and design, which significantly reduce the number of variables required in prediction down to three, V_{LIP}, *k2*, and *k2end*. In the meantime, uncertainties from identification, prediction, and modelling are minimized to a moderate level. As an outcome, the PIP predictions are accurate with a median of 1.76 cmH_2O for a superset predictions of 623 cases in prior study [56]. Furthermore, most of the physiological relevant features are preserved and can be used for further study (*k2* and *k2end* to show the stiffness of patient lungs, and can be used to calculate an overdistension metric to estimate the risk of harm [46]).

In the real world, it is hard to simulate and predict the exact evolution of physiological variables for multiple reasons, such as variable patient-specific dynamics and evolution (V_{LIP} changes over PEEP in **Figure 9**), identification and prediction errors, model structural errors, and lack of understanding of the underlying process [37]. In addition, the human body is a precise and complex system where numerous factors function all together. Therefore, a successful predictive model should balance model complexity (simplification), robustness, and accuracy, while preserving physiological information as much as possible. As model complexity increases, robustness can drop, with no better prediction outcome and the risk of overfitting or loss of physiological relevance based on the model structure and approaches employed.

Therefore, when designing a model for biological system, moderate simplification of the studied process should be considered for robustness consideration for model performance and prediction accuracy. Meanwhile, keeping physiologically relevant features (curvature features in HLM) also contributes to increasing robustness for prediction performance, and enhance the underlying mechanics as well. Furthermore, moderate errors for variables values (including prediction errors) can be tolerated to minimize the unpredictable variability of

human dynamics.

5 Conclusion

This study presents a detailed error analysis for the identification and prediction procedure of a clinically validated digital twin model for mechanical ventilation. While overall prediction errors are very accurate for the volume control case presented, as well as in pressure control, the underlying causes of this accuracy were not understood. The error analysis and analysis of its propagation presented in making clinically relevant predictions involve many forms of inter-related and often inseparable errors. The overall results delineate the elements and model structure areas where error is both highest and lowest relative to the potential total error based on summing each element. The result shows the model analyzed is robust to a range of uncertainties. Finally, this study offers a better picture of how multiple errors and uncertainties (in data, parameters/variables estimation, prediction, and model structure) are involved in this lung mechanics model with moderate complexity, and thus yield advice for model design. More importantly, the approach taken is generalizable to the growing number of digital twin models emerging for biomedical clinical decision support and provide a means of verifying the cause of good, or poor, model prediction errors, which in turn can provide confidence in these models and both their capabilities and their limitations.

6 Acknowledgement

This work was supported the Service Public Fédéral Stratégie et Appui (BOSA) – DIGITWIN4PH, and H2020 MSCA Rise (#872488 DCPM, [https://ec.europa.eu]). The authors also acknowledge support from Nature Science Foundation of China (NSFC) with Grant No 12102362.

7 REFERENCES

1. Chase JG, Preiser JC, Dickson JL, Pironet A, Chiew YS, Pretty CG, *et al.* Next-generation, personalised, model-based critical care medicine: a state-of-the art review of in silico virtual patient models, methods, and cohorts, and how to validation them. *BioMedical Engineering OnLine* 2018; **17**(1): 24. DOI: 10.1186/s12938-018-0455-y.
2. Gani A, Gribok AV, Rajaraman S, Ward WK, Reifman J. Predicting subcutaneous glucose concentration in humans: data-driven glucose modeling. *IEEE Transactions on Biomedical Engineering* 2008; **56**(2): 246–254.
3. Laviola M, Bates DG, Hardman JG. Mathematical and Computational Modelling in Critical Illness. *European Respiratory & Pulmonary Diseases* 2019; **5**(1).
4. Major VJ, Chiew YS, Shaw GM, Chase JG. Biomedical engineer's guide to the clinical aspects of intensive care mechanical ventilation. *BioMedical Engineering OnLine* 2018; **17**(1): 169. DOI: 10.1186/s12938-018-0599-9.
5. Gattinoni L, Marini JJ, Collino F, Maiolo G, Rapetti F, Tonetti T, *et al.* The future of mechanical ventilation: lessons from the present and the past. *Critical Care* 2017; **21**(1): 183. DOI: 10.1186/s13054-017-1750-x.
6. Sundaresan A, Chase JG, Shaw GM, Chiew YS, Desaive T. Model-based optimal PEEP in mechanically ventilated ARDS patients in the Intensive Care Unit. *BioMedical Engineering OnLine* 2011; **10**(1): 64. DOI: 10.1186/1475-925X-10-64.
7. Tawhai MH, Bates JH. Multi-scale lung modeling. *J Appl Physiol (1985)* 2011; **110**(5): 1466–1472. DOI: 10.1152/japplphysiol.01289.2010.
8. Damanhuri NS, Chiew YS, Othman NA, Docherty PD, Pretty CG, Shaw GM, *et al.* Assessing respiratory mechanics using pressure reconstruction method in mechanically ventilated spontaneous breathing patient. *Comput Methods Programs Biomed* 2016; **130**: 175–185. DOI: 10.1016/j.cmpb.2016.03.025.
9. Tawhai MH, Burrowes KS. Multi-scale models of the lung airways and vascular system. *Adv Exp Med Biol* 2008; **605**: 190–194. DOI: 10.1007/978-0-387-73693-8_33.
10. Hickling KG. The Pressure–Volume Curve Is Greatly Modified by Recruitment. *American Journal of Respiratory and Critical Care Medicine* 1998; **158**(1): 194–202. DOI: 10.1164/ajrccm.158.1.9708049.
11. Rees SE. The Intelligent Ventilator (INVENT) project: The role of mathematical models in translating physiological knowledge into clinical practice. *Computer Methods and Programs in Biomedicine* 2011; **104**: S1–S29.
12. C. Schranz, C. Knöbel, J. Kretschmer, Z. Zhao, K. Möller. Hierarchical Parameter Identification in Models of Respiratory Mechanics. *IEEE Transactions on Biomedical Engineering* 2011; **58**(11): 3234–3241. DOI: 10.1109/TBME.2011.2166398.
13. Steimle KL, Mogensen ML, Karbing DS, Bernardino de la Serna J, Andreassen S. A model of ventilation of the healthy human lung. *Computer Methods and Programs in Biomedicine* 2011; **101**(2): 144–155. DOI: https://doi.org/10.1016/j.cmpb.2010.06.017.
14. Bates JH. Lung mechanics--the inverse problem. *Australas Phys Eng Sci Med* 1991; **14**(4): 197–203.
15. Burrowes KS, De Backer J, Smallwood R, Sterk PJ, Gut I, Wirix-Speetjens R, *et al.* Multi-scale computational models of the airways to unravel the pathophysiological mechanisms in asthma and chronic obstructive pulmonary disease (AirPROM). *Interface Focus* 2013; **3**(2): 20120057. DOI: 10.1098/rsfs.2012.0057.
16. Burrowes KS, Swan AJ, Warren NJ, Tawhai MH. Towards a virtual lung: multi-scale, multi-physics modelling of the pulmonary system. *Philosophical Transactions Series A, Mathematical, Physical, and Engineering Sciences* 2008; **366**(1879): 3247. DOI: 10.1098/rsta.2008.0073.
17. Burrowes KS, Hunter PJ, Tawhai MH. Anatomically based finite element models of the human pulmonary arterial and venous trees including supernumerary vessels. *Journal of Applied Physiology* 2005; **99**(2): 731–738. DOI: 10.1152/japplphysiol.01033.2004.
18. Tawhai MH, Clark AR, Chase JG. The Lung Physiome and virtual patient models: From morphometry to clinical translation. *Morphologie* 2019; **103**(343): 131–138. DOI: 10.1016/j.morpho.2019.09.003.
19. Morton SE, Knopp JL, Chase JG, Docherty P, Howe SL, Möller K, *et al.* Optimising mechanical ventilation through model-based methods and automation. *Annual Reviews in Control* 2019; **48**: 369–382. DOI: https://doi.org/10.1016/j.arcontrol.2019.05.001.
20. Neelakantan S, Xin Y, Gaver DP, Cereda M, Rizi R, Smith BJ, *et al.* Computational lung modelling in

respiratory medicine. *Journal of the Royal Society Interface* 2022; **19**(191). DOI: 10.1098/rsif.2022.0062.
21. Barahona J, Sahli Costabal F, Hurtado DE. Machine learning modeling of lung mechanics: Assessing the variability and propagation of uncertainty in respiratory-system compliance and airway resistance. *Computer Methods and Programs in Biomedicine* 2024; **243**: 107888. DOI: 10.1016/j.cmpb.2023.107888.
22. Chase JG, Zhou C, Knopp JL, Moeller K, Benyo B, Desaive T, *et al.* Digital Twins and Automation of Care in the Intensive Care Unit. *Cyber–Physical–Human Systems*, John Wiley & Sons, Ltd; 2023. DOI: 10.1002/9781119857433.ch17.
23. Bates JHT. *Lung Mechanics: An Inverse Modeling Approach*. Cambridge: Cambridge University Press; 2009. DOI: 10.1017/CBO9780511627156.
24. Schranz C, Docherty PD, Chiew YS, Chase JG, Möller K. Structural identifiability and practical applicability of an alveolar recruitment model for ARDS patients. *IEEE Transactions on Biomedical Engineering* 2012; **59**(12): 3396–3404.
25. Caljé-van der Klei T, Sun Q, Chase JG, Zhou C, Tawhai MH, Knopp JL, *et al.* Pulmonary response prediction through personalized basis functions in a virtual patient model. *Computer Methods and Programs in Biomedicine* 2024; **244**: 107988. DOI: 10.1016/j.cmpb.2023.107988.
26. Sun Q, Chase JG, Zhou C, Tawhai MH, Knopp JL, Möller K, *et al.* Over-distension prediction via hysteresis loop analysis and patient-specific basis functions in a virtual patient model. *Computers in Biology and Medicine* 2021; **141**: 105022. DOI: https://doi.org/10.1016/j.compbiomed.2021.105022.
27. Sun Q, Chase JG, Zhou C, Tawhai MH, Knopp JL, Möller K, *et al.* Prediction and estimation of pulmonary response and elastance evolution for volume-controlled and pressure-controlled ventilation. *Biomedical Signal Processing and Control* 2022; **72**: 103367. DOI: https://doi.org/10.1016/j.bspc.2021.103367.
28. Zhou C, Chase JG, Knopp J, Sun Q, Tawhai M, Möller K, *et al.* Virtual patients for mechanical ventilation in the intensive care unit. *Computer Methods and Programs in Biomedicine* 2021; **199**: 105912. DOI: https://doi.org/10.1016/j.cmpb.2020.105912.
29. Morton SE, Knopp JL, Tawhai MH, Docherty P, Heines SJ, Bergmans DC, *et al.* Prediction of lung mechanics throughout recruitment maneuvers in pressure-controlled ventilation. *Computer Methods and Programs in Biomedicine* 2020; **197**: 105696. DOI: https://doi.org/10.1016/j.cmpb.2020.105696.
30. Mirams GR, Pathmanathan P, Gray RA, Challenor P, Clayton RH. Uncertainty and variability in computational and mathematical models of cardiac physiology. *The Journal of Physiology* 2016; **594**(23): 6833–6847. DOI: 10.1113/JP271671.
31. Maier HR, Tolson BA. Sensitivity and Uncertainty. In: Jørgensen SE, Fath BD, editors. *Encyclopedia of Ecology*, Oxford: Academic Press; 2008. DOI: 10.1016/B978-008045405-4.00230-5.
32. Arslan J, Benke KK, Samarasinghe G, Sowmya A, Guymer RH, Baird PN. Model Structure Uncertainty in the Characterization and Growth of Geographic Atrophy. *Translational Vision Science & Technology* 2021; **10**(6): 2. DOI: 10.1167/tvst.10.6.2.
33. Gupta A, Govindaraju RS. Propagation of structural uncertainty in watershed hydrologic models. *Journal of Hydrology* 2019; **575**: 66–81. DOI: 10.1016/j.jhydrol.2019.05.026.
34. Pathak R, Ragheb H, Thacker NA, Morris DM, Amiri H, Kuijer J, *et al.* A data-driven statistical model that estimates measurement uncertainty improves interpretation of ADC reproducibility: a multi-site study of liver metastases. *Scientific Reports* 2017; **7**(1): 14084. DOI: 10.1038/s41598-017-14625-0.
35. Wu JL, Levine ME, Schneider T, Stuart A. Learning about structural errors in models of complex dynamical systems. *Journal of Computational Physics* 2024; **513**: 113157. DOI: 10.1016/j.jcp.2024.113157.
36. Xiu D, Sherwin SJ. Parametric uncertainty analysis of pulse wave propagation in a model of a human arterial network. *Journal of Computational Physics* 2007; **226**(2): 1385–1407. DOI: 10.1016/j.jcp.2007.05.020.
37. Li H, Wu J. Uncertainty analysis in ecological studies. *Scaling and Uncertainty Analysis in Ecology: Methods and Applications Edited by J Wu, KB Jones, H Li, and OL Loucks Springer, Dontrecht, The Netherlands* 2006: 45–67.
38. Zhu D, Peng DZ, Cluckie ID. Statistical analysis of error propagation from radar rainfall to hydrological models. *Hydrology and Earth System Sciences* 2013; **17**(4): 1445–1453. DOI: 10.5194/hess-17-1445-2013.
39. Guillard V, Guillaume C, Destercke S. Parameter uncertainties and error propagation in modified atmosphere packaging modelling. *Postharvest Biology and Technology* 2012; **67**: 154–166. DOI: 10.1016/j.postharvbio.2011.12.014.
40. Yuan H, Suki B, Lutchen KR. Sensitivity Analysis for Evaluating Nonlinear Models of Lung Mechanics. *Annals of Biomedical Engineering* 1998; **26**(2): 230–241. DOI: 10.1114/1.117.

41. Wang A, Cao S, Aboelkassem Y, Valdez-Jasso D. Quantification of uncertainty in a new network model of pulmonary arterial adventitial fibroblast pro-fibrotic signalling. *Philosophical Transactions Series A, Mathematical, Physical, and Engineering Sciences* 2020; **378**(2173): 20190338. DOI: 10.1098/rsta.2019.0338.
42. Paun LM, Colebank MJ, Olufsen MS, Hill NA, Husmeier D. Assessing model mismatch and model selection in a Bayesian uncertainty quantification analysis of a fluid-dynamics model of pulmonary blood circulation. *Journal of the Royal Society Interface* 2020; **17**(173): 20200886. DOI: 10.1098/rsif.2020.0886.
43. Karimzadeh R, Fatemizadeh E, Arabi H, Zaidi H. Prediction Error Propagation: A Novel Strategy to Enhance Performance of Deep Learning Models in Seminal Segmentation. *2021 IEEE Nuclear Science Symposium and Medical Imaging Conference (NSS/MIC)*, *2021 IEEE Nuclear Science Symposium and Medical Imaging Conference (NSS/MIC)*. 2021. DOI: 10.1109/NSS/MIC44867.2021.9875890.
44. Colebank MJ, Umar Qureshi M, Olufsen MS. Sensitivity analysis and uncertainty quantification of 1-D models of pulmonary hemodynamics in mice under control and hypertensive conditions. *International Journal for Numerical Methods in Biomedical Engineering* 2021; **37**(11): e3242. DOI: 10.1002/cnm.3242.
45. Jansen MJW. Prediction error through modelling concepts and uncertainty from basic data. *Nutrient Cycling in Agroecosystems* 1998; **50**(1): 247–253. DOI: 10.1023/A:1009748529970.
46. Sun Q, Chase JG, Zhou C, Tawhai MH, Knopp JL, Möller K, *et al.* Non-invasive over-distension measurements: data driven vs model-based. *Journal of Clinical Monitoring and Computing* 2022. DOI: 10.1007/s10877-022-00900-7.
47. Zhou C, Chase JG, Sun Q, Knopp J, Tawhai MH, Desaive T, *et al.* Reconstructing asynchrony for mechanical ventilation using a hysteresis loop virtual patient model. *BioMedical Engineering OnLine* 2022; **21**(1): 16. DOI: 10.1186/s12938-022-00986-9.
48. Stahl CA, Möller K, Schumann S, Kuhlen R, Sydow M, Putensen C, *et al.* Dynamic versus static respiratory mechanics in acute lung injury and acute respiratory distress syndrome. *Crit Care Med* 2006; **34**(8): 2090–2098. DOI: 10.1097/01.Ccm.0000227220.67613.0d.
49. The ARDS Definition Task Force*. Acute Respiratory Distress Syndrome: The Berlin Definition. *JAMA* 2012; **307**(23): 2526–2533. DOI: 10.1001/jama.2012.5669.
50. Zhou C, Chase JG, Rodgers GW, Tomlinson H, Xu C. Physical Parameter Identification of Structural Systems with Hysteretic Pinching. *Computer-Aided Civil and Infrastructure Engineering* 2015; **30**(4): 247–262. DOI: 10.1111/mice.12108.
51. Fisher JB, Mammel MC, Coleman JM, Bing DR, Boros SJ. Identifying lung overdistention during mechanical ventilation by using volume-pressure loops. *Pediatric Pulmonology* 1988; **5**(1): 10–14. DOI: 10.1002/ppul.1950050104.
52. Grasso S, Terragni P, Mascia L, Fanelli V, Quintel M, Herrmann P, *et al.* Airway pressure-time curve profile (stress index) detects tidal recruitment/hyperinflation in experimental acute lung injury. *Crit Care Med* 2004; **32**(4): 1018–1027.
53. Jandre FC, Modesto FC, Carvalho AR, Giannella-Neto A. The endotracheal tube biases the estimates of pulmonary recruitment and overdistension. *Medical & Biological Engineering & Computing* 2008; **46**(1): 69–73. DOI: 10.1007/s11517-007-0227-5.
54. J. J. Marini, P. S. Crooke 3rd, J. D. Truwit. Determinants and limits of pressure-preset ventilation: a mathematical model of pressure control. *Journal of Applied Physiology* 1989; **67**(3): 1081–1092. DOI: 10.1152/jappl.1989.67.3.1081.
55. Nayyerloo M, Chase JG, Zhou C, Rabiepour M. Real-time structural health monitoring of nonlinear hysteretic structures using a fast and slow dynamics separation method. *IFAC Journal of Systems and Control* 2021; **15**: 100122. DOI: 10.1016/j.ifacsc.2020.100122.
56. Sun Q, Chase JG, Zhou C, Tawhai MH, Knopp JL, Möller K, *et al.* Impact of Two Lung Elastance Identification Methods on Pulmonary Mechanics Prediction. *IFAC-PapersOnLine* 2021; **54**(15): 97–102. DOI: https://doi.org/10.1016/j.ifacol.2021.10.238.